Detection of small drizzle droplets in a large cloud chamber using ultra high-resolution radar

Zeen Zhu[1], Fan Yang[1], Pavlos Kollias[1,2], Raymond A. Shaw[3], Alex B. Kostinski[3], Steve Krueger[4], Katia Lamer[1], Nithin Allwayin[3], Mariko Oue[2]

[1]Brookhaven National Laboratory, Upton, NY, USA
[2]Stony Brook University, Stony Brook, NY, USA
[3]Michigan Technological University, Houghton, MI, USA
[4]University of Utah, Salt Lake City, UT, USA

Corresponding author: Zeen Zhu (zzhu1@bnl.gov)

Abstract

A large convection cloud chamber has the potential to produce drizzle-sized droplets, thus offering a new opportunity to investigate aerosol-cloud-drizzle interactions at a fundamental level under controlled environmental conditions. One key measurement requirement is the development of methods to detect the low concentration drizzle drops in such a large cloud chamber. In particular, remote sensing methods may overcome some limitations of in situ methods.

Here, the potential of an ultra-high-resolution radar to detect the radar return signal of a small drizzle droplet against the cloud droplet background signal is investigated. It is found that using a small sampling volume is critical to drizzle detection in a cloud chamber to allow a drizzle drop in the radar sampling volume to dominate over the background cloud droplets signal. For instance, a radar volume of 1 cubic centimeter (cm^3) would enable the detection of drizzle embryos with diameter larger than 40 μm. However, the probability of drizzle sampling also decreases as the sample volume reduces, leading to a longer observation time. Thus, the selection of radar volume should consider both of the signal power and the drizzle occurrence probability. Finally, observations from the Pi Convection-Cloud Chamber are used to demonstrate the single drizzle particle detection concept using small radar volume. The results presented in this study also suggest new applications of ultra-high-resolution cloud radar for atmospheric sensing.

1. Introduction

Drizzle formation is one of the most important microphysical processes in warm clouds. Yet the processes controlling drizzle formation remain poorly understood (Wood, 2012). The most challenging aspect is the initial formation of drizzle embryos with diameter around 30 μm ~ 50 μm. The formation of small drizzle particles in this range can neither be adequately explained by the traditionally-defined condensation growth process nor by the traditionally-defined collision-coalescence (C-C) process owing to their low efficiency (Yau and Rogers, 1996;Pruppacher and Klett, 2012;Falkovich et al., 2006;Beard and Ochs III, 1993). Several mechanisms have been hypothesized to explain the efficiency of these processes including i) fine-scale turbulence in cloud (Pinsky and Khain, 1997;Shaw, 2003); ii) giant cloud condensation nuclei (GCCN) (Johnson, 1982;Feingold et al., 1999); and iii) longwave cooling (Roach, 1976;Harrington et al., 2000). Nevertheless, it remains unclear to which extent these proposed mechanisms can adequately explain the origin of drizzle embryos.

One main barrier that hinder our ability to investigate the drizzle initiation process is the lack of observations with sufficient sensitivity and spatiotemporal resolution to detect the early growth of drizzle particles. As such an instrumented large convection cloud chamber with well-controlled initial and boundary conditions might help to improve our understanding of the drizzle initiation mechanism (Shaw et al., 2020). Unlike other types of chambers, a convection-cloud chamber can generate a steady state cloud system for hours in a turbulent environment by maintaining a warm saturated bottom surface, a cold saturated top surface, and a constant aerosol injection rate (Chang et al., 2016). The Michigan Tech Pi convection chamber with a dimension of 2 m x 2 m x 1 m (width x depth x height) has been used to explore aerosol-cloud-turbulence interactions, however, the Pi Chamber is too small to initiate drizzle embryos mainly due to the relatively short lifetime of cloud droplets therein. Results from large eddy simulations indicate that drizzle can be initiated in a large convection-cloud chamber with a height on the order of 10 m (Thomas et al., 2023). However, the drizzle drops are sparse in a large chamber, so the detection of single drizzle embryos in a large cloud chamber is challenging for in-situ probes that generally have a sampling volume of only a few cubic centimeters. On the other hand, active remote sensors have the ability to rapidly sample large volumes and thus offer an attractive option for the detection of small drizzle droplets in a cloud chamber.

82

Here, we will demonstrate that the detection of an individual drizzle droplet in the presence of numerous cloud droplets is possible with a radar that can achieve a very small sampling volume. The detection of individual drizzle droplets is possible because the radar signal-to-noise ratio (SNR) of a point target (drizzle droplet) is not affected by the radar observational volume, while the SNR of a distributed target (cloud droplets) scales with the radar volume. In the following sections, the detection limits of an individual drizzle particle are investigated using idealized particle size distributions and real particle size distributions from the Michigan Tech Pi Chamber. In the end, the potential of THz radars offering unprecedented sub-centimeter range resolution will be discussed for developing the single drizzle detection radar (Cooper and Chattopadhyay, 2014).

93

94

2. Drizzle detection using radar

96

The detection of early drizzle particles in clouds has been the topic of extensive research. First, the radar needs to have sufficient sensitivity to detect cloud and drizzle droplets. This is typically accomplished using millimeter-wavelength radar (Kollias et al., 2007). Early methodologies for the detection of drizzle drop in clouds employ the use of reflectivity thresholds, ranging from −15 to −20 dBZ, to identify drizzle existence (Frisch et al., 1995;Liu et al., 2008;Comstock et al., 2004). Kollias et al. (2011) introduced the use of the radar Doppler spectra skewness as a more sensitive method for detecting the presence of small drizzle droplets (Acquistapace et al., 2017;Zhu et al., 2022). The radar Doppler spectra technique improved the detection of drizzle droplets that can produce as low as -30 dBZ (Zhu et al., 2022).

106

However, the use of the radar Doppler spectra technique in a cloud chamber is challenging. First, this will require that the radar point vertically to take advantage of the differential velocity between cloud and drizzle droplets. If we assume a monodisperse droplet size distribution (DSD) and Rayleigh scattering conditions, a drizzle detection limit of -30 dBZ is equivalent to a concentration of 10^{-3} cm^{-3} of drizzle droplets with diameter equal to 100 μm or a concentration of 6.4×10^{-2} cm^{-3} of drizzle droplets with 50 μm diameter. In the former case, the drizzle particle size is quite

113   large and not quite an early drizzle droplet detection. In the latter case, the concentration of drizzle

114   droplets is much higher than the concentration observed in nature ($\sim 10^{-4}\ cm^{-3}$) (Zhu et al., 2022).

115   Furthermore, the conventional cloud radar has range resolution of tens of meters, which is not

116   applicable in a chamber facility which may be on the order of several meters (approaching the

117   collision mean free path).

118

119   As a result, we consider alternative methods to increase the probability of early drizzle droplet

120   detection against the cloud droplet signal. As the number concentration of drizzle particle is low,

121   by applying a small radar sampling volume V_{Radar}, it is possible that only one drizzle droplet is

122   presence in V_{Radar}. In this case, the drizzle particle can be considered as a point target with

123   backscattering cross section $\sigma(m^2)$ and the received radar echo power P_r (mW) is commonly

124   expressed as (Battan, 1973):

125

$$P_{r,drizzle} = P_t \frac{G^2 \lambda^2}{(4\pi)^3 r^4} \sigma(D_d) \tag{1}$$

127

128   where P_t is the transmit peak power (mW), G is the antenna gain, r (m) is the range of the target

129   relative to the radar receiver and λ (m) is the radar wavelength. It is noteworthy that P_r for a point

130   target does not depend on the radar sampling volume V_{Radar}. For distributed targets such as a cloud

131   droplet population described by a droplet size distribution (DSD) that represents the number

132   concentration of cloud droplets as a function of diameter, the received radar echo power is given

133   by:

134

$$P_{r,cloud} = P_t \frac{G^2 \lambda^2}{(4\pi)^3 r^4} \cdot V_{Radar} \cdot \sum_{i=0}^{n} N_c(D_i)\sigma(D_i)\Delta D_i \tag{2}$$

136

137   Where n is the number of cloud droplets in the radar volume and $N_c(D)$ is the DSD with units of

138   m^{-4}. In this case, the received radar echo power depends on the radar sampling volume, which is

139   given by the following expression:

$$V_{Radar} = \pi \left(\frac{r\theta_{3dB}}{2}\right)^2 \cdot \Delta R \tag{3}$$

where θ_{3dB} is antenna radiation pattern 3-dB beamwidth in radians and ΔR is the range resolution. Assuming Rayleigh scattering, the backscatter cross section of the drizzle and cloud droplets is proportional to the sixth power of the particle diameter and inversely proportional to the fourth power of the wavelength ($\sigma(D) \sim D^6/\lambda^4$). Combing Eq. 1 and Eq. 2, the ratio of radar received echo power from drizzle and cloud is given by the following expression:

$$\frac{Signal}{Background} = \frac{P_{r,drizzle}}{P_{r,cloud}} = \frac{1}{V_{Radar}} \cdot \frac{D_d^6}{\sum_{i=0}^{n} N_c(D_i) D_i^6 \Delta D_i}. \tag{4}$$

Eq. 4 indicates that the probability of detecting a single drizzle droplet in the radar sampling volume increases inversely to the radar sampling volume (point vs distributed target).

3. Detection requirement

Here, we will evaluate how small the radar sampling volume needs to be to detect drizzle drops with different diameters against three background (cloud) conditions: i) monodisperse cloud DSD, ii) cloud DSD from a theoretical model and iii) observed cloud DSD from the Michigan Tech Pi Chamber. For simplicity, we will assume that a drizzle drop is detectable if its radar return power is equal to that of the background echo contributed from cloud droplets.

3.1. Monodisperse cloud DSD

We first construct an idealized scenario by considering two categories of droplets, i.e. cloud droplet with a diameter of D_c and a single drizzle drop with a diameter of D_d, the number concentration of cloud droplets in the radar sampling volume is N_c (m^{-3}).

In this case, Eq. 4 is simplified as:

$$\frac{Signal}{Background} = \frac{1}{V_{Radar}} \cdot \frac{D_d{}^6}{N_c \cdot D_c^6} \qquad (5)$$

When the signal power equals to the background, the radar sampling volume enabling single drizzle particle detection is estimated as a function of the size ratio $x = \frac{D_d}{D_c}$ shown in Fig. 1. The results are shown for various cloud droplet concentrations. It is noted that the required radar volume for detection depends on the drizzle drop size and the cloud number concentration. Larger radar volume would be required for drizzle detection as the particle size ratio increase; for a given particle size ratio, decreasing cloud number concentration can enhance the required radar volume. For example, if the cloud number concentration is 50 cm^{-3} and the mean cloud diameter (D_c) is 20 μm, then the detection of a drizzle particle with diameter of 40 μm ($x = 2$) requires radar volume around 1 cm^3. Such sampling volume are not achievable with traditional radar systems that employ sampling volumes of the order of 1000 m^3 or more (Kollias et al., 2016).
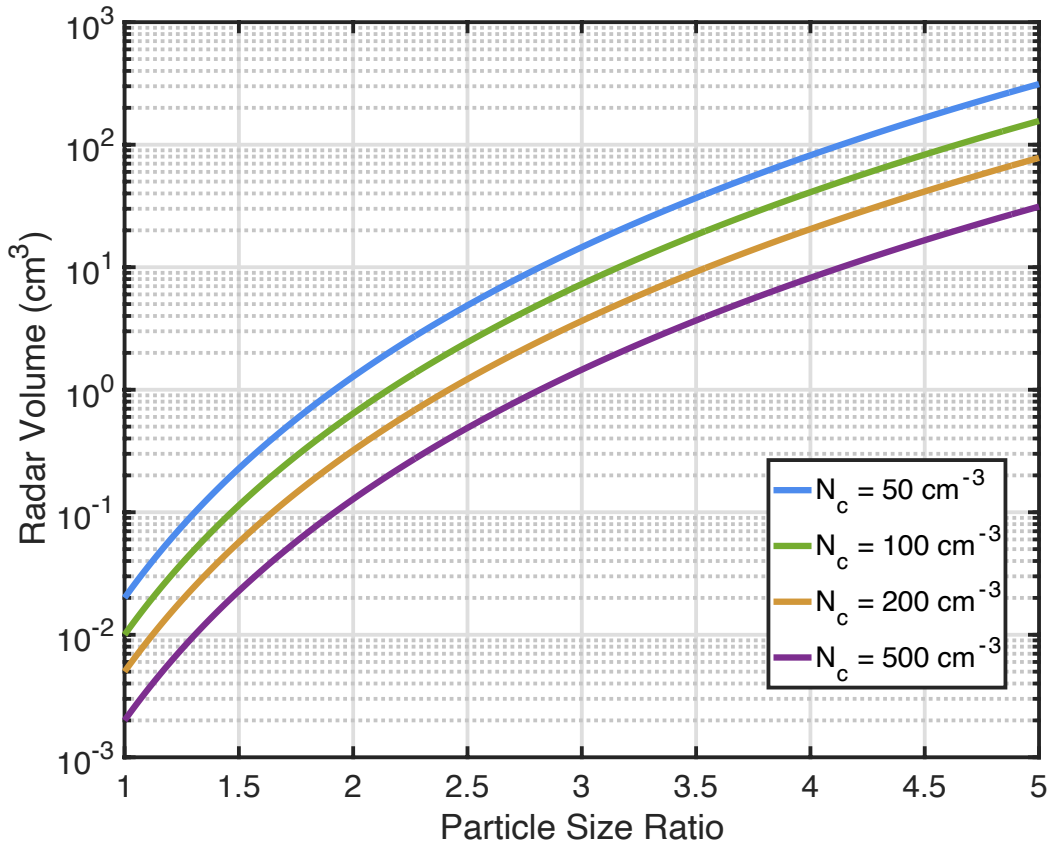
184   Figure 1: Radar observational volume for single-drizzle-drop detection as a function of particle

185   size ratio $x = \frac{D_d}{D_c}$. Lines of different color represent clouds number concentration (N_c): $50\ cm^{-3}$

186   (blue), $100\ cm^{-3}$ (green), $200\ cm^{-3}$ (yellow) and $500\ cm^{-3}$ (purple).

187

188

189   ## 3.2 Drizzle detection against an idealized cloud droplet background

190

191   In a realistic cloud chamber environment, we expect a population of cloud droplets with various

192   sizes that can be represented by a DSD. Particularly, when condensation and fallout are the main

193   sources and sinks for the evolution equation for the DSD, the DSD in the cloud chamber can be

194   approximately described by theoretically derived distributions (Saito et al., 2019;Chandrakar et al.,

195   2020;Krueger, 2020). Here we adapt the theoretical DSD formula derived by Krueger (2020) to

196   investigate the ability of a radar to detect a drizzle embryo present in a small sample volume under

197   different chamber environment conditions. To better represent the cloud DSD under different

198   environments, the analytical DSD is rearranged to be expressed as a function of liquid water

199   content (LWC$_c$; $g\ m^{-3}$) and number concentration (N_c; m^{-3}) as:

200

201
$$N(D_c) = \frac{2N_c D_c}{\pi^{1/2}} \left(\frac{4\Gamma\left(\frac{5}{4}\right)\pi^{\frac{1}{2}}\rho_l N_c}{3LWC_c} \right)^{2/3} \exp\left(-\left(\frac{4\Gamma\left(\frac{5}{4}\right)\pi^{\frac{1}{2}}\rho_l N_c}{3LWC_c} \right)^{\frac{4}{3}} \left(\frac{D_c}{2}\right)^4 \right) \qquad (6)$$

202

203   where ρ_l is liquid water density ($g\ m^{-3}$), and D_c is cloud droplet diameter (m). $N(D_c)$ represents

204   the number concentration of cloud droplet for the given diameter ($cm^{-3}\ \mu m^{-1}$).

205

206   Here we define the minimal drizzle drop ($D_{d,min}$) as the size of particle with radar return power

207   equal to the total return power from cloud droplets in a given radar volume (V). Given the cloud

208   DSD described by Eq. 6, $D_{d,min}$ can be estimated as:

209

210
$$D_{d,min}^6 = \int V N(D_c) D_c^6 dD \qquad (7)$$
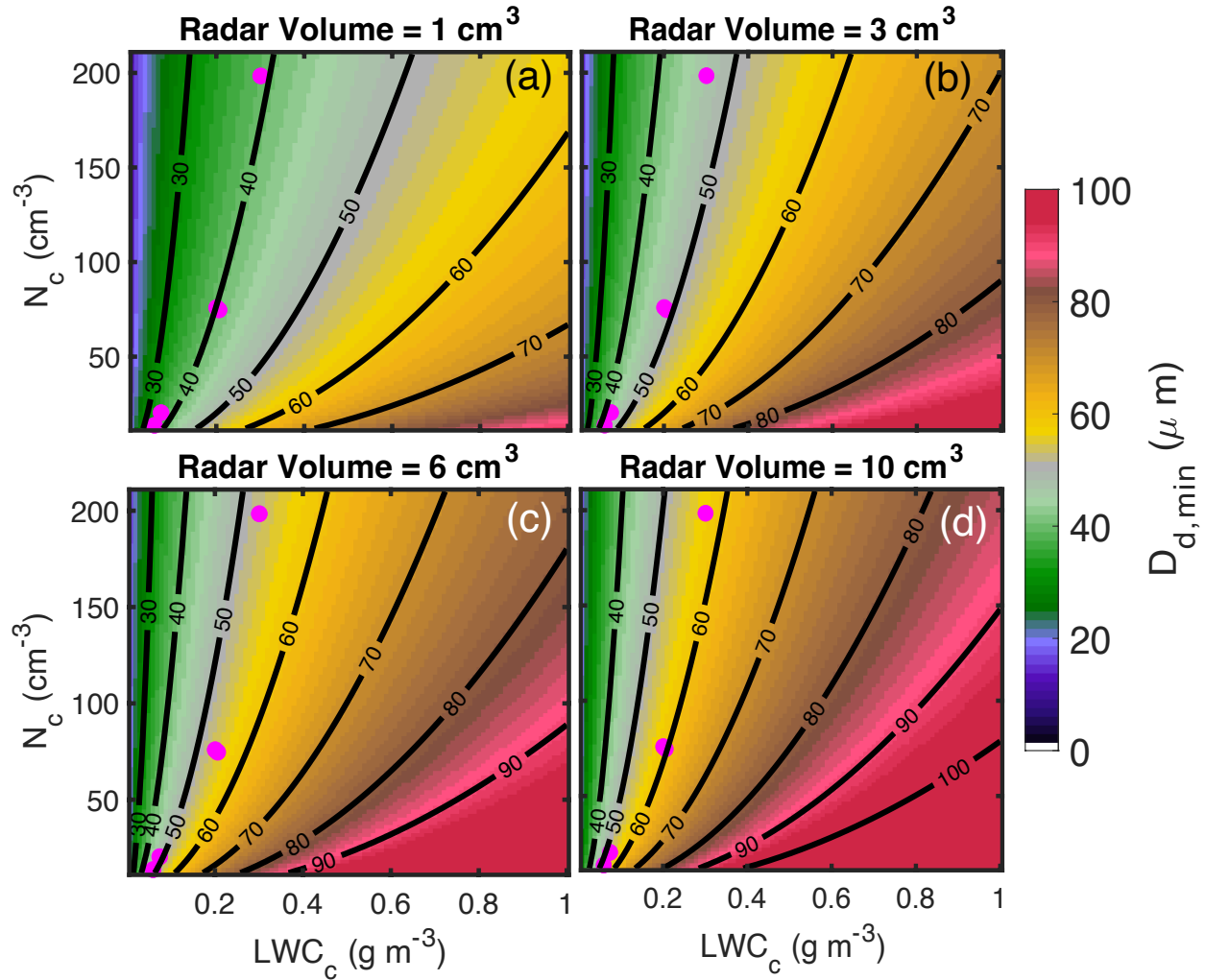
Figure2: The minimal detectable drizzle particle ($D_{d,min}$) under different LWC_c and N_c conditions with radar sampling volume of (a) 1 cm^3, (b) 3 cm^3, (c) 6 cm^3 and (d) 10 cm^3. The black lines are the $D_{d,min}$ contour of 30 μm, 40 μm, 50 μm, 60 μm, 70 μm. The magenta dots indicate the LWC_c and N_c observed in the Pi-cloud chamber.

Fig. 2 illustrates $D_{d,min}$ under different LWC_c and N_c combinations for various radar volumes. For a given steady-state cloud in a convection chamber (i.e., fixed LWC_c and N_c), $D_{d,min}$ generally increases as the radar volume increases. This is because larger radar volumes contain more cloud droplets that produce stronger background power, thus only a larger drizzle particle with a higher backscattering signal would be detectable. On the other hand, for a given radar observational volume, $D_{d,min}$ is jointly determined by LWC_c and N_c which are inversely proportional. As such,

223 $D_{d,min}$ increases rapidly with increasing LWC$_c$ but slightly decreases with increasing N_c. This

224 contrasting relationship is caused by a larger sensitivity of radar reflectivity to particle size than to

225 number concentration. Thus, increasing LWC$_c$ can increase mean cloud particle size and greatly

226 enhance the background power, leading to a larger detectable $D_{d,min}$. On the other side, when

227 LWC$_c$ is fixed, increasing cloud total number concentration tends to decrease particle size. The

228 reduced cloud particle size would reduce the backscattering power and more than compensate for

229 the power enhancement contributed from the increased number concentration.

230

231 It should be noted that LWC_c and N_c in a convection cloud chamber have a stronger correlation

232 compared with those in atmospheric clouds (Shaw et al., 2023). Instead, the LWC$_c$ and N_c often

233 exhibit a positive covariance relationship. To understand the typical value of these two quantities

234 in the chamber environment, we refer to typical measurement data from the Pi Chamber (magenta

235 dots in Fig. 2). The data are from experiments conducted by Chandrakar et al. (2018). We can

236 notice that for this specific experiment set up, drizzle embryos with diameter ranging from 40 μm

237 to 60 μm can be detected using radar observational volume from 1 cm^3 to 10 cm^3.

238

239 The aforementioned estimation is conducted under the assumption that signal (drizzle) power is

240 equal to the background (cloud) power. In practice, to reduce the detection false alarms, the drizzle

241 signal should be larger than the backgrounds. Here we define the signal to noise ratio (SNR) to

242 investigate the drizzle detectability in the chamber environment:

243

244
$$SNR = 10\,log10\left(\frac{D_d^6}{\int VP(D_c)D_c^6\,dD}\right). \tag{8}$$

245

246 Fig. 3 shows the estimated SNR for four drizzle particles under varying LWC$_c$ and N_c conditions

247 with a radar volume of 1 cm^3. Generally, a smaller LWC$_c$ and a larger N_c correspond to a large

248 SNR, which is preferable for drizzle detection. If we arbitrarily choose SNR > 3 as the detection

249 threshold, to detect a drizzle drop with diameter of 50 μm in a radar volume of 1 cm^3 (Fig. 3c),

250 LWC$_c$ in the cloud chamber should be lower than 0.3 $g\ m^{-3}$ and N_c should be high than 90 cm^{-3}.

251 The required LWC$_c$ and N_c would be different for different drizzle particle targets: to detect drops

252 with diameter of 60 μm , LWC$_c$ should be lower than 0.5 $g\ m^{-3}$ and N_c should be higher than 90

253 cm^{-3}. It should be noted that although a drizzle drop is more likely to be detected by the radar at a

254 lower LWC$_c$, drizzle initiation is generally more likely to occur at a higher LWC$_c$ because the

255 collision-coalescence rate is thought to be proportional to the square of LWC (Kostinski and Shaw,

256 2005). This suggests appropriate LWC$_c$ and N_c combinations should be achieved such that drizzle

257 can form by the C-C process in a convection cloud chamber and it can also be detected by radar in

258 a small sampling volume. It is also noted that the results shown in Fig.3 are based on a radar

259 volume of 1 cm^3, and the estimated *SNR* would change if a different radar volume size is applied.

260 For instance, increasing the radar volume will enhance the background power thus decreasing the

261 *SNR* for the given cloud chamber environment.
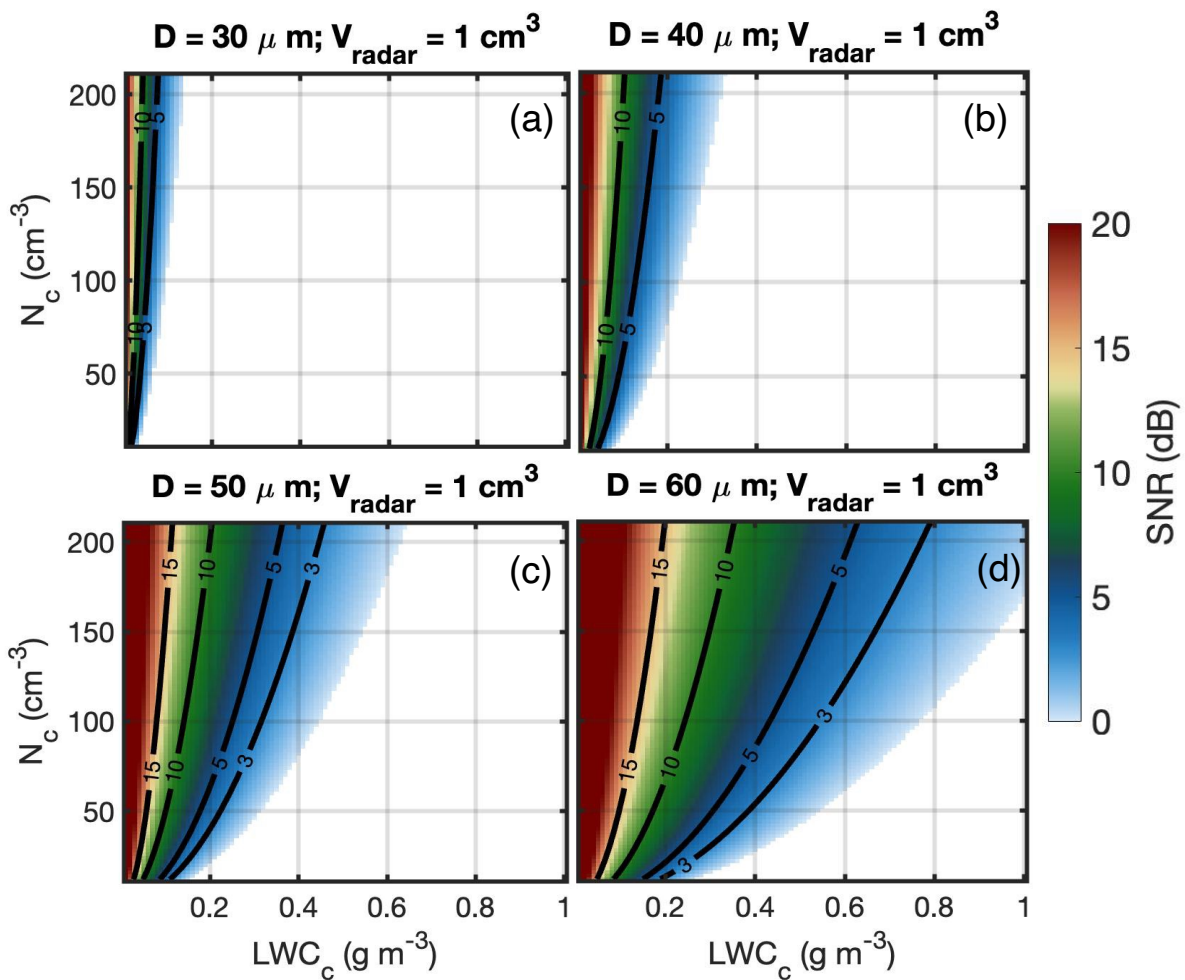
262

263 Figure 3: SNR of the drizzle signal under different LWC and *N* conditions in a 1 cm^3 radar sample

264 volume for drizzle diameters of 30 μm, 40 μm, 50 μm, 60 μm. The black lines are SNR contours

265 of 3 dB, 5 dB, 10 dB and 15 dB. SNR lower than 0 is indicated as the blank region.

266

267

268   ## 4. Probability of detection due to drizzle concentration

269

270   In the previous section, it was demonstrated that a radar with very small sampling volume ($\sim cm^3$)

271   can plausibly achieve the detection of single drizzle droplets against a cloud background signal.

272   On the other hand, the smaller the radar volume, the lower the probability of a drizzle particle

273   encountering the volume. To illustrate this trade-off scenario, we define the probability of drizzle

274   occurrence in the radar volume ($p(D_d)$) as:

275

276
$$p(D_d) = \begin{cases} 1, & VN(D_d)\Delta D \geq 1 \\ VN(D_d), & VN(D_d)\Delta D < 1 \end{cases} \tag{9}$$

277

278   Specifically, the product of V and $N(D_d)$ represents the expected number of drizzle drops in the

279   radar volume. If the product is smaller than 1, it indicates the probability of the occurrence of

280   drizzle particle in a given volume; while if the product is larger than 1, it means, statistically, at

281   least one drizzle drop with a diameter of D_d exists in the radar volume, and thus we set $p(D_d)=1$.

282

283

284
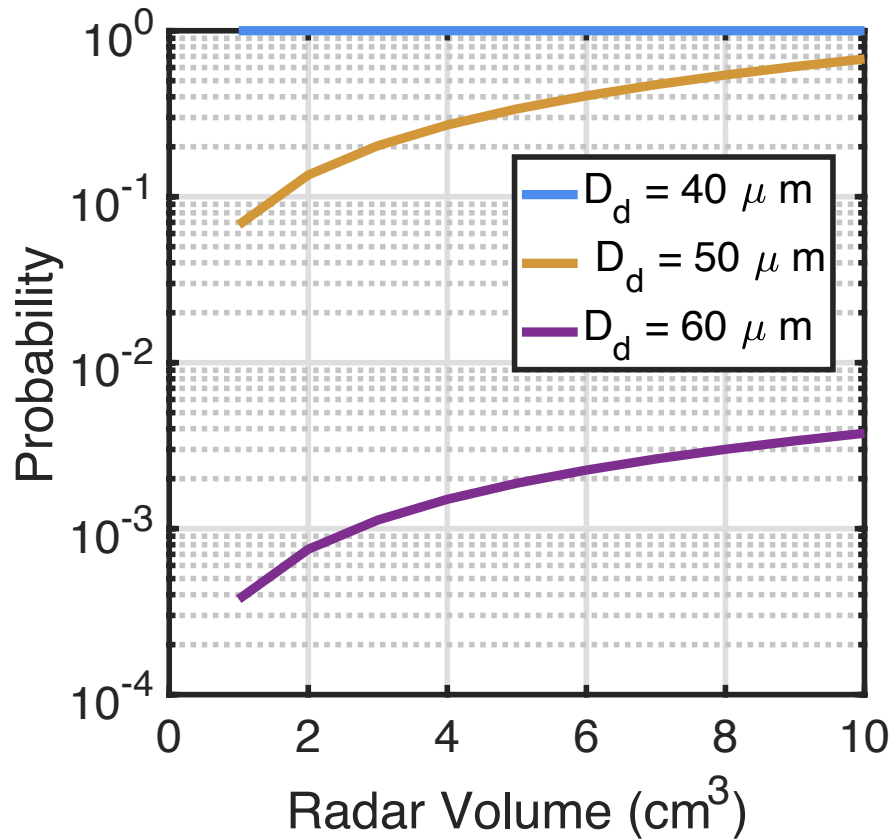
Figure 4: The probability of drizzle occurrence as a function of radar observational volume. The blue, yellow, and purple lines indicate the drizzle particle with diameters of 40 μm, 50 μm, and 60 μm.

288

The probability of occurrence for three selected drizzle particles as a function of radar volume is shown in Fig. 4. The $N(D)$ in Eq. 9 is adapted from the size distribution described by Eq.6, with LWC$_c$ and N_c set as 0.5 g m^{-3} and 50 cm^{-3}, respectively. For these conditions, drizzle droplets with a diameter of 40 μm have sufficiently high concentration to be on average always present in volumes larger than 1 cm^3. For drizzle droplets with a diameter of 50 μm or 60 μm, their concentration is low enough that their probability of being found in a 10 cm^3 volume is on average below 1. It is also noticed that the occurrence probability is strongly sensitive to the particle size: the probability of drizzle with 60 μm diameter occurring in the volume is almost two magnitudes smaller than that for a particle with 50 μm diameter. A smaller drizzle occurrence in the volume

298 indicates that a larger number of radar samples would be required to find one particle, leading to

299 a longer observational time.

300

301 The probability of a drizzle drop to be in the radar sampling volume or passing through the radar

302 volume within a finite time period should be an important consideration for a practical

303 measurement system. Fig. 5 shows the probability of the occurrence of drizzle particle under

304 different chamber environments same as Fig. 3. The blank region in Fig. 5 indicates the

305 corresponding SNR shown in Fig. 3 is lower than 0 (i.e., cannot be detected by the radar even they

306 exist in the sampling volume). Generally, it is noticed that the probability of occurrence differs in

307 various chamber environment for different droplet size: large droplets have lower occurrence

308 probability under small LWC and high N conditions.
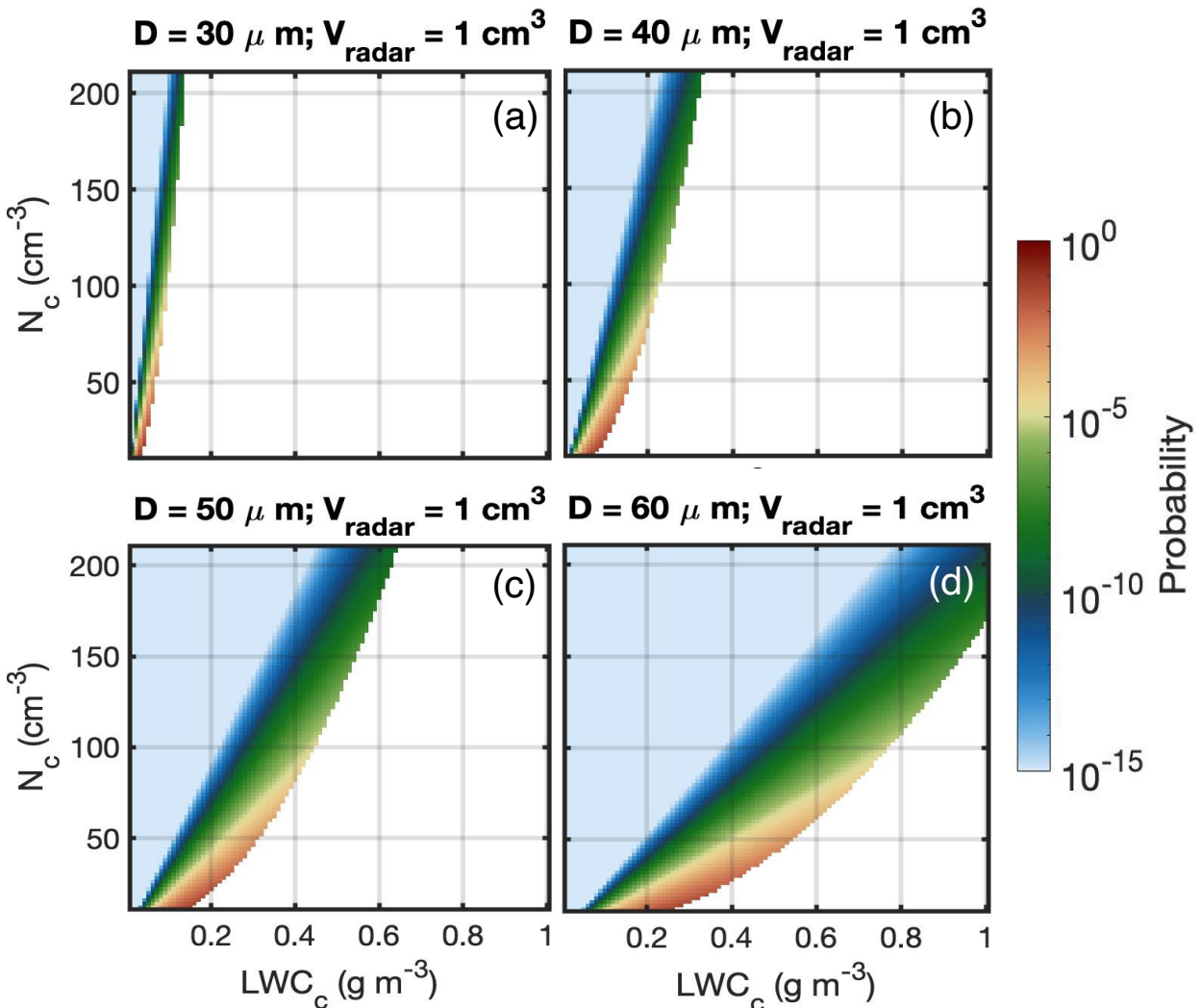
309   Figure 5: Drizzle occurrence probability under different LWC and N conditions for a 1 cm^3 radar

310   volume with particle diameter of (a) 30 μm, (b) 40 μm, (c) 50 μm, and (d) 60 μm. The blank region

311   indicates that the associated SNR is smaller than 0 (Fig. 3).

312

313   Comparison of Fig. 3 and Fig. 5 reveals that conditions that favor high radar SNR (i.e., larger drops

314   or smaller radar sampling volume) are associated with a lower probability of occurrence of the

315   drizzle droplet in the radar volume and subsequently increase the radar sampling time. For example,

316   to detect a drizzle particle of 50 μm diameter under the condition of LWC_c and N_c of 0.3 g m^{-3}, 90

317   cm^{-3}, the particle occurrence probability is on the magnitude of 10^{-8} (Fig. 5c) for SNR equals to 3

318   (Fig. 3c). A 1 dB enhancement of SNR threshold would decrease the occurrence probability to 10^{-11}.

319   ^{11}. This implies that on average, a volume of air equal to 10^{11} times the size of the radar sampling

320   volume needs to be sampled before a drizzle droplet will be detected. Assuming an air mean flow

321   within the cloud chamber of 1 m s^{-1}, this implies that a radar sampling volume with a typical

322   dimension of 1 cm will be updated (through advection) 100 times per second. If the radar is

323   sampling along 1000 range gates (i.e. assuming a chamber with height of 10 m), this suggests that

324   the radar can sample a volume equal to 10^5 its radar sampling volume each second. To reach the

325   average required sampling volume (10^{11}), it will take 10^6 seconds or 11.5 days. This is an

326   unrealistically long observational time. For practical application, we want to work with sampling

327   configurations that will not require to sample more than 10^9 times the radar sampling volume (~10s

328   of minutes).

329

330   Another factor to consider in estimating the probability of drizzle occurrence with a certain

331   diameter in a specific volume is the realism of using Eq. 6 for describing the $N(D)$ in a cloud

332   chamber. Eq. 6 describes the cloud droplet distribution controlled by the condensation process

333   alone, thus the results may underestimate the actual drizzle occurrence as condensation is

334   inefficient to produce large drizzle particle. In nature or in a large convection cloud chamber, the

335   C-C mechanism is expected to be a more efficient process to increase the size and concentration

336   of drizzle droplets.

337

338   Here we apply the ClusColl model to demonstrate that Fig. 4 and Fig. 5 may underestimate the

339   drizzle occurrence probability with the collision-coalescence process being activate. ClusColl is a

340   simulation method for describing droplet motions and collisions in turbulent flows (Krueger and

341   Kerstein, 2018). ClusColl simulates the movement of individual droplets in a vertical column due

342   to turbulence and gravitational sedimentation. The unique capability of the ClusColl model is its

343   capability to efficiently simulate the droplet collisions and coalescence process. Fig. 6 shows the

344   simulated DSD with and without the collision-coalescence process for a 10-*m*-height cloud

345   chamber and with cloud number concentration of 100 cm^{-3}. The temperature difference between

346   top and bottom walls is 40 °C. Noticeable differences can be identified at the right tail of the

347   distribution, particularly for droplet diameter larger than 40 μm: more larger droplets are generated

348   if the collision-coalescence process is active. The higher concentration of large drops results in a

349   significantly shorter waiting time for detection compared to what was calculated for the

350   condensation-only examples given in the earlier part. For instance, for the generated particle with

351   diameter of 50 μm, the C-C process can generate number concentration more than 100 higher than

352   the one without C-C process included. Reviewing the earlier estimation, to detect drizzle particle

353   with diameter of 50 μm with SNR higher than 4, the required 10^6 s becomes 10^4 s which is

354   approximately 3 hours, which is much more achievable for laboratory experiment. Thus, the

355   estimation based on the condensation-only distribution (Eq. 6) is the most-conservative scenario.

356   The actual radar measurement time would likely to be much shorter when the C-C process is

357   activated.

358

359
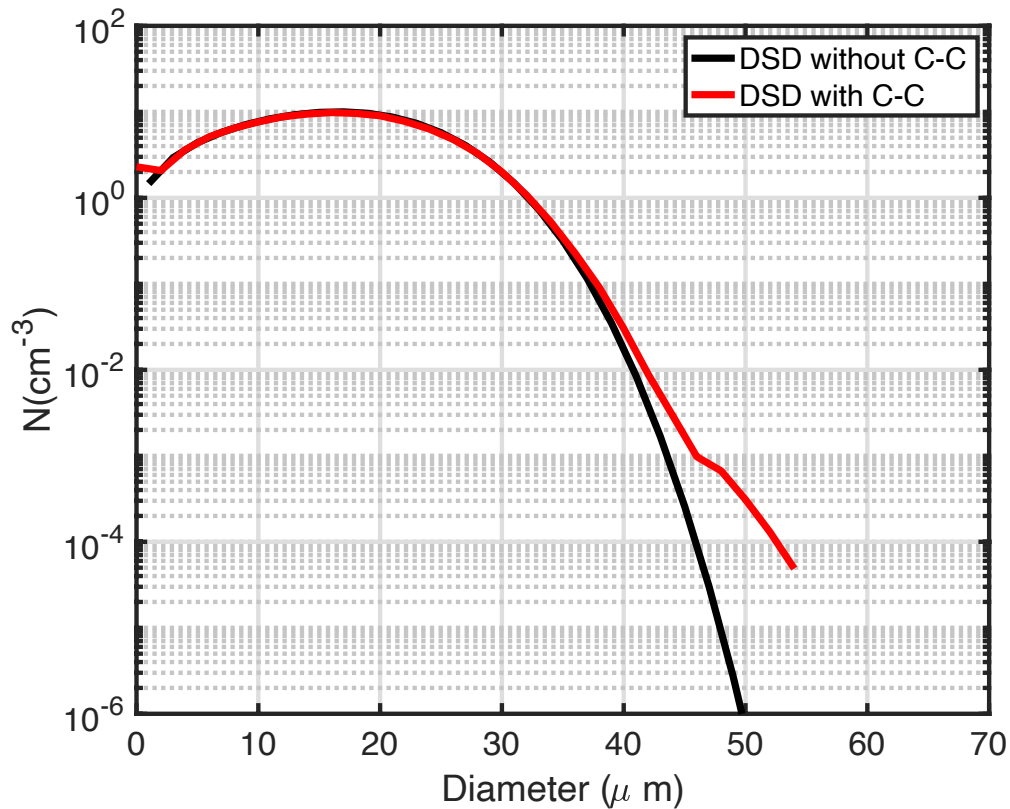
360

361

362   Figure 6: DSD simulated from the ClusColl model with (red line) and without (black line) droplet

363   growth by collision-coalescence. In both cases, growth by condensation in a uniform

364   supersaturation field, and removal by size-dependent droplet sedimentation are calculated.

365   Therefore, the black line is described by the distribution given by Equation 6.

366

367

368

369   5. Evaluation from cloud chamber observations

370

371   In a cloud chamber and in the real atmosphere, the DSD in the radar sampling volume is expected

372   to be time dependent due to turbulent fluctuations. To better quantify the particle backscattering

373   power and its fluctuation in a small volume, observations made in the Pi Chamber using a

374   holographic system (Holo-Pi) are used. Holo-Pi uses the principle of in-line digital holography to

375 measure the spatial distribution and sizes of cloud particles (Fugal and Shaw, 2009;Beals et al.,

376 2015), and is specifically designed for the Pi-chamber environment (Desai et al., 2018). In contrast

377 to the typical measurement strategy of single particle detections requiring time averaging, Holo-

378 Pi captures instantaneous snapshots of all cloud droplets in the sample volume of 3.6 cm^3 (0.6 cm

379 × 0.6 cm × 10 cm) and is well suited to measure the temporal variations of cloud droplet

380 populations within a sample volume similar to plausible radar sample volumes. The inability to

381 resolve the smallest cloud droplets in the size distribution is not expected to be a significant

382 limitation as the backscattering radar power is more sensitive to larger particle diameters. For the

383 results presented here, cloud droplets are formed in the Pi Chamber by activation of size-selected

384 sodium chloride aerosol particles (dry particle diameter ≈ 130 nm) injected into a supersaturated

385 turbulent flow sustained by an unstable temperature difference of 20 K. An illustration of the 3D

386 view of the cloud droplets measured by Holo-Pi at different time instants in the Pi-chamber is

387 shown in Fig. 7. The sample volume used for our calculations is limited to a vertical extent of 5

388 cm as particle detectability falls off beyond this point; this results in a total sample volume of 1.8

389 cm^3. The Holo-Pi system is set up to capture a hologram every 10 seconds during a 720-s period.

390 For the optical configuration used here, the Holo-Pi has a lower size resolution of 12 μm

391 throughout its sample volume.

392

393

394
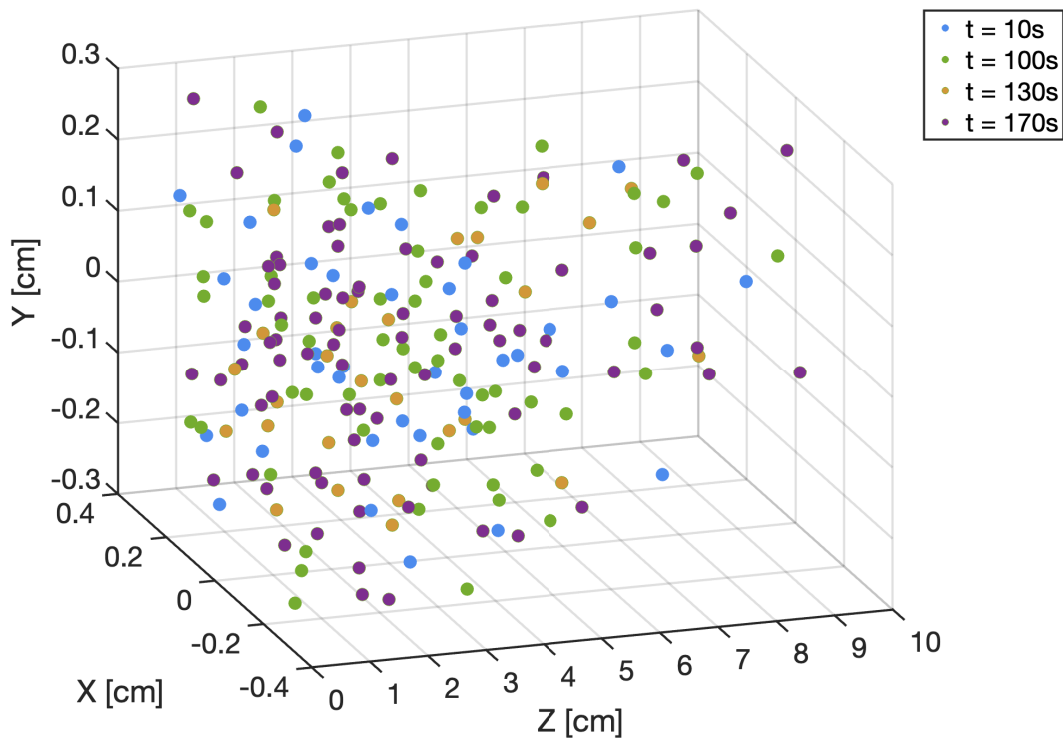
395

396 Figure 7: A 3D view of the particle locations observed by Holo-Pi in the Pi Chamber. Different

397 colors represent observations taken at different timesteps.

398

399 The Holo-Pi observational volume is divided into five sub volumes with the cross section of 0.36

400 cm^2 and the depth increasing from 1 to 5 cm with an increment of 1 cm, thus, corresponding to a

401 volume of 0.36, 0.72, 1.08, 1.44 and 1.8 cm^3. Within each sub-volume at each time step, the total

402 backscattering cross section for the detected droplets is estimated using a THz radar with

403 wavelength of 0.44 mm. The calculated radar backscattering cross section as a function of volume

404 size is shown in Fig. 8. Similar to the previous estimation, we see that the background power

405 increases with volume size due to the increment of cloud droplets. Importantly, the uncertainty

406 bars shown in Fig. 8 represent the standard deviation of the backscattering cross section during the

407 observational time, which indicates the background power fluctuations. We notice that the cloud

408 distribution in a small radar sampling volume is highly heterogeneous in time, and the magnitude

409 of the background fluctuation varies by approximately a factor of 10. In order to detect drizzle

410 drops, the backscattering power of the drizzle drop should be larger than the range of background

411   fluctuations. For example, a radar volume smaller than $0.36\ cm^3$ should be utilized to detect a

412   droplet with a diameter larger than $22\ \mu m$, and a radar sampling volume smaller than $1\ cm^3$ is

413   needed to detect droplet with diameter larger than $30\ \mu m$ for this particular Pi Chamber experiment

414   set up.

415
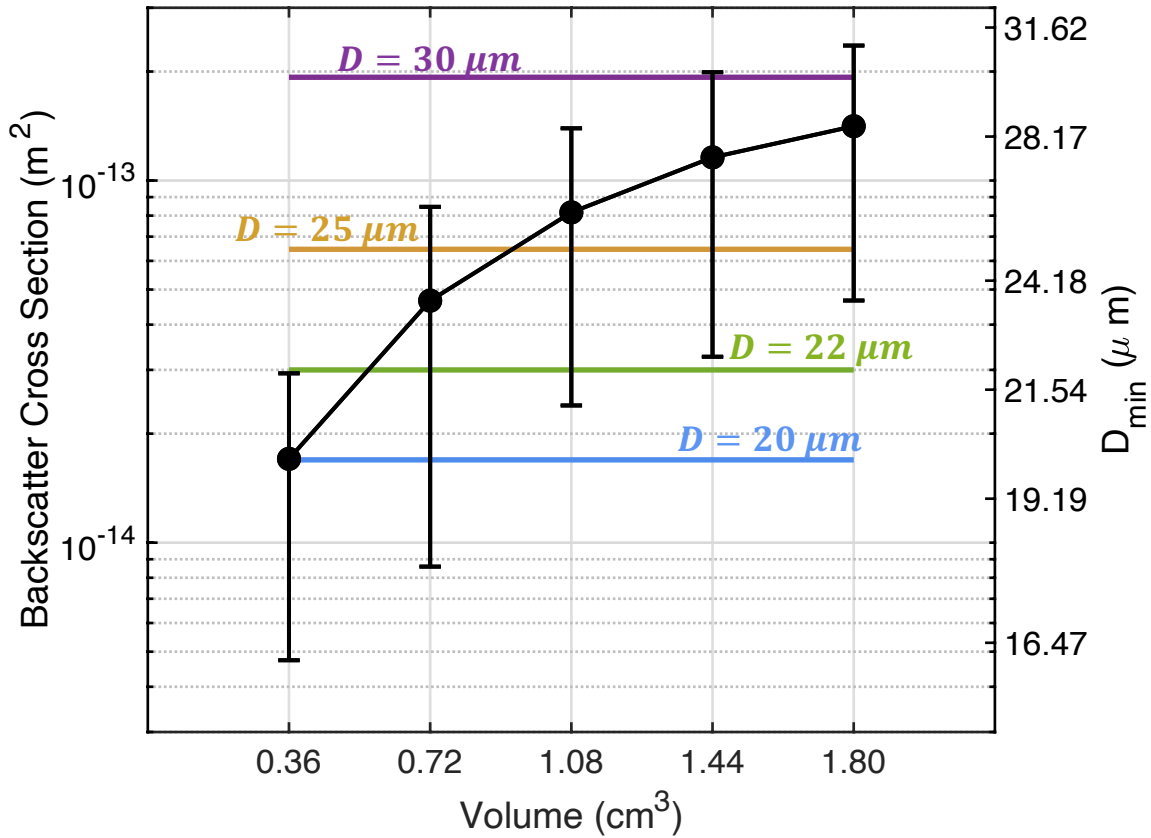
416

417   Figure 8: Dots and uncertainty bars indicate the mean and standard deviation of the total

418   backscattering cross-section (with units of m^2) of droplets measured in different volumes by Holo-

419   Pi during the observational period. The right axis and the horizontal lines represent the diameter

420   of a single drizzle drop with backscattering power equivalent to the background.

421 To further demonstrate the single drizzle detection concept using a small radar volume, a pseudo-
422 radar observation experiment is conducted based on the Holo-Pi measurements. The Holo-Pi
423 observational volume is divided into 4 sub-volumes indicated as different lines shown in Fig. 9. In
424 each volume, we consider the mean radar backscattering power from all cloud particles sampled
425 during the observational period as the background noise, and the power estimated at each time step
426 as the signal, such that the SNR as a function of observation time is estimated. To simulate the
427 drizzle occurring events, artificial drizzle droplets with diameter of 30 μm, 40 μm, 50 μm are
428 added to the volume at 200 s, 400 s, and 600 s, respectively, and the associated SNR is estimated.
429 Fig. 9 shows a clear SNR enhancement when the drizzle droplets are added. The signal
430 enhancement is more significant when using a small sampling volume and for larger drizzle drop
431 diameter, which is consistent with the theoretical estimation in Sec. 3. For instance, a drizzle drop
432 with a diameter of 50 μm can have a SNR of 23 dB with a volume of 0.36 cm^3 while it has a SNR
433 of 15 dB with a volume of 1.44 cm^3. For a drizzle drop of 30 μm, the SNR with a volume of 0.36
434 cm^3 can reach to 10 dB, which is an adequate SNR value for radar detection, while with a volume
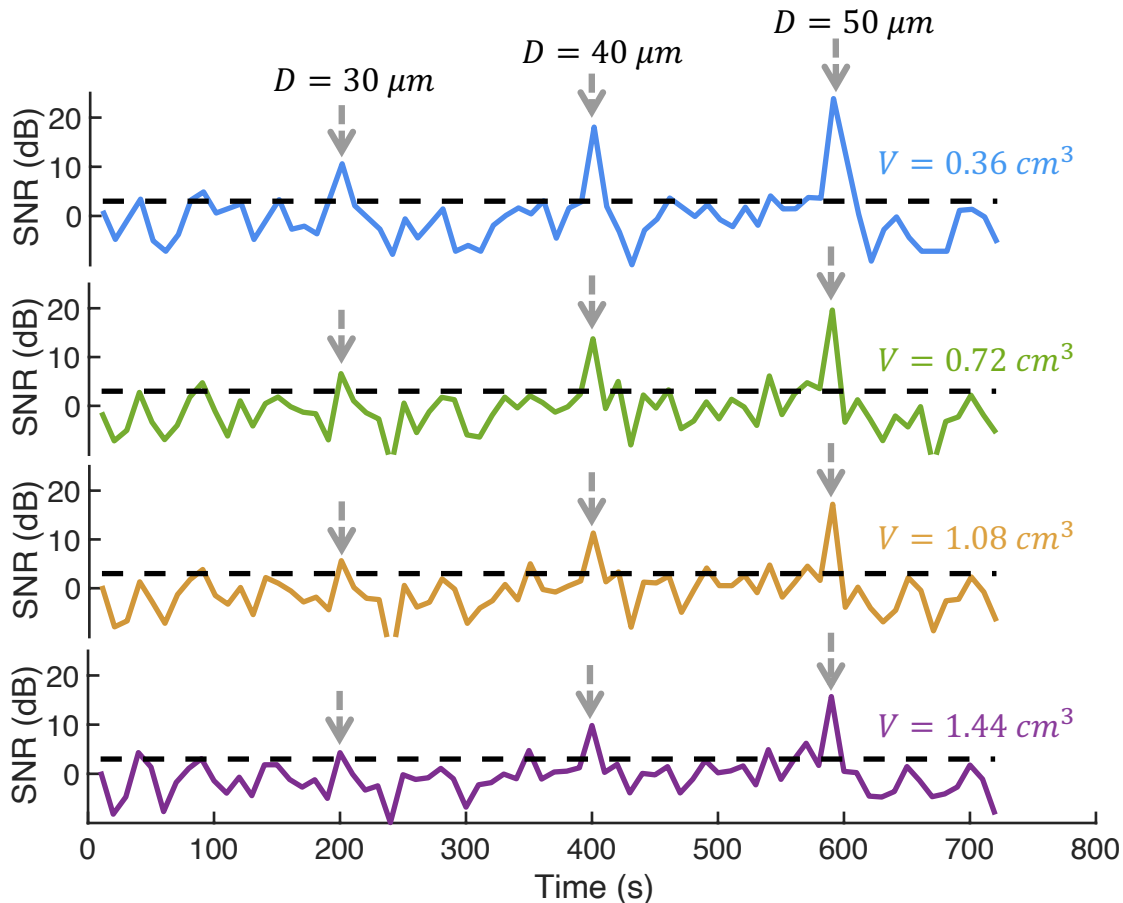
435   of 1.44 cm^3, the drizzle drop SNR is overwhelmed by background fluctuation and it is unable to
436   be detected.

437

438   Figure 9: Simulated SNR of radar measurements during the Holo-Pi observational period using
439   four sampling volumes: 0.36 cm^3(blue line), 0.72 cm^3(green line), 1.08 cm^3 (yellow line) and
440   1.44 cm^3 (purple line). The grey arrows indicate an artificial drizzle particle is added at the
441   indicated time step. The black dashed line indicates a SNR of 3, which is used as a threshold to
442   distinguish the signal (drizzle) from the background (clouds) in Fig. 3.

443

444   6. Summary

445

446   Recent simulation results suggest that drizzle initiation could occur in a large convection-cloud
447   chamber. Such a facility would provide measurements in a controlled environment that can
448   advance our understanding of warm rain formation in clouds. One of the critical measurements in
449   a large convection-cloud chamber is the detection of low-concentration drizzle droplets in the
450   presence of numerous cloud droplets. Early in the drizzle initiation, those drizzle drops are rare
451   and in-homogeneously distributed in the chamber, presenting a significant detection challenge for
452   conventional in-situ probes. Here, the potential of a radar with ultra-fine sampling volume for
453   drizzle detection is investigated. It was demonstrated that if the radar sampling volume becomes
454   orders of magnitude smaller (e.g., several cm^3), compared to those typically available in research
455   radars ($\sim10^3$-10^6 m^3), isolated drizzle particles can be detected against the cloud background signal.
456   This concept is based on the notion that the SNR of point targets (i.e., drizzle droplet) is
457   independent of the radar sampling volume while the SNR of background (i.e., high concentration
458   cloud droplets) scales with the sampling volume.

459

460   A theoretical DSD was adapted to represent the distribution of cloud droplets in a convection cloud
461   chamber and to estimate properties of a detectable drizzle particle. It was shown that the minimum
462   size of an isolated drizzle droplet that can be detected with such a radar depended on the radar
463   sampling volume and the strength of the background signal (i.e., cloud droplets radar return), that
464   in turn, depends on LWC and N_c. To minimize the false alarm drizzle detection, we require that
465   the backscattering power from a drizzle particle should be larger than the backscattered power

466 contributed from the cloud particles (SNR>1). It is demonstrated that the application of a small

467 radar volume can significantly enhance SNR under a given chamber environment. On the other

468 hand, the smaller the radar sampling volume the lower the probability of an isolated drizzle droplet

469 to be sampled. Thus, the determination of the radar volume for drizzle detection should account

470 for the size of drizzle particle of interest, the environment conditions that favor drizzle initiation

471 and the required observational time.

472

473 In addition to analytical estimates, real observations from the MTU Pi convection-cloud chamber

474 are used to demonstrate the single drizzle particle detection framework. The Holo-Pi system(Desai

475 et al., 2018) is applied to provide detailed 3D imaging of the cloud particles in the cloud chamber,

476 from which the fluctuations of the backscattering power in a small volume can be well estimated.

477 Generally, the observational results are consistent with the theoretical estimation showing that the

478 background power is decreased and the ability to detect drizzle particles is enhanced as radar

479 sample volume is decreased. It is also noticed that the magnitude of the background fluctuation is

480 comparable to the mean power, which indicate that the distribution of cloud droplets is highly

481 inhomogeneous in the small volume. Thus, the power from a drizzle particle should at least

482 dominate the background power fluctuation in order to be detected. With the cloud chamber

483 environment from the experiment, drizzle particles with diameter larger than 30 μm can be

484 confidently detected using a radar sampling volume of 1 cm^3 or lower.

485

486 The key remaining question is the technological feasibility of building a radar that can operate

487 within a box (large convection cloud chamber) and achieve the required ultra-fine range resolution.

488 In fact, the effort of using "small" radar volumes for single particle detection has already been

489 achieved in previous studies. For example, Schmidt et al. (2012) utilized a C-band radar with a 14-

490 m^3 observational volume and successfully detected the trajectories of rain droplet with diameter

491 down to 0.5 mm. In our case, the required radar sampling volume for drizzle detection is much

492 smaller (with several cm^3). Such ultra-fine range resolution can be achieved using a THz radar

493 operating at 340 or 680 GHz that can support wide bandwidth waveforms and thus enable sub-

494 centimeter range resolution (Cooper and Chattopadhyay, 2014). If the radar operates at a very high

495 carrier frequency (THz) it can afford a very wide bandwidth for pulse modulation. In this case, the

496 range resolution in not dictated by the pulse length but from the radar bandwidth (Cooper and

497 Chattopadhyay, 2014). The ultra-fine range resolution along with a reflector that minimizes the

498 angular spread of the radar beam can result in radar sampling volumes of a few cm^3. Such radar

499 imaging capabilities have been extensively used for security screening at airports, for example. In

500 our context, additional complexity is introduced by the fact that this radar needs to operate in a

501 chamber with typical dimension of ~ 10 m. These technical design issues will be the focus of a

502 follow-up paper study that will include real observations of drizzle droplets from a THz radar

503 system.

504

505 To conclude, we outline three issues that will need to be properly addressed before a radar can be

506 applied to the drizzle-detection problem in a cloud chamber:

507

508 1) Does the radar have enough sensitivity to detect a single drizzle particle? With the

509 development of the THz technology, radar with centimeter resolution is achievable,

510 however, the currently developed THz radars are mainly used to detect relatively hard

511 targets that do not require ultra-high sensitivity. For the purpose of drizzle detection,

512 however, the backscattering cross-section is on the order of 10^{-13} m^2; such lower receiving

513 power would require the radar to have a much higher transmitting power or a larger antenna

514 size. Fortunately, an advantage for the drizzle detection in a cloud chamber is that the radar

515 detection range is only several meters depending on the size of the chamber. According to

516 Eq. 1, radar receiving power is inversely proportional to the fourth power of the target

517 distance. Thus, the small detection range may greatly relieve the demand for high

518 sensitivity in the radar design. In addition, recent advancements in THz transmitters allow

519 us to utilize higher power output transmitter (~50 to 200 mW) at THz frequencies such as

520 340 GHz.

521

522 2) What are the appropriate radar sampling strategies for drizzle detection in a cloud chamber

523 facility? Most of the cloud radars applied in the atmosphere are vertically pointing and can

524 provide continuous observation at a given location along the radar beam. However as

525 discussed in the paper, drizzle occurrence in the chamber is extremely rare and

526 inhomogeneous in space and time. If the radar is vertically pointing, with the radar beam

527 of several cm width, it may wait significant time for the radar to detect one drizzle drop.

528   Adding a scanning capability to the radar may provide a more efficient way to observe and
529   detect drizzle in the cloud chamber.

530

531 3) How to eliminate or reduce the degradation effect of the chamber environment on a radar
532   signal? In particular, the cloud chamber is a humid environment with liquid particles
533   continually falling towards the bottom. Accumulation of water on the radar antenna can
534   also severally attenuate the transmitting power and degrade the radar detectability.
535   Furthermore, the chamber walls and the in-situ instruments mounted inside would produce
536   strong backscattering signals and pollute the backscattering signal from hydrometeors.
537   Thus, the design of the radar should also account for radar instrument design and sampling
538   strategies that minimize these noise sources so that the best possible detection capability
539   can be achieved.

540

541 In short, this paper demonstrates the conceptual feasibility of THz radars for rare drizzle detection
542 in a laboratory context. Undoubtedly, the development of a high-resolution radar for drizzle
543 detection in a cloud chamber needs close collaborations between cloud physics scientists and radar
544 engineers moving forward.

545

546 **Competing interests.**

547 **P. K.** is an associate editor of AMT and the peer-review process was handled by an independent
548 editor. The authors have no other competing interests to declare.

549

550 **Code/Data availability**

551 The codes and observations used to conduct all the analyses in this study are available upon
552 request.

553
554

Author contributions

Zeen Zhu conceptualized and implemented the method, performed the analysis, produced the figures, and wrote the initial draft of the manuscript. Pavlos Kollias and Fan Yang contributed to the conceptualization and provide guidance on the analysis. Raymond A. Shaw and Alex B. Kostinski contributed to the simplified model described in Section 3.1. Steve Krueger provided the ClusColl model. Nithin Allwayin provided the Holo-Pi measurements from the Pi Chamber. All authors read the manuscript draft and contributed comments and manuscript editing.

Acknowledgements

Authors from Brookhaven National Laboratory were supported by the Office of Biological and Environmental Research in the Department of Energy, Office of Science, through the United States Department of Energy Contract No. DE-SC0012704. Authors from Michigan Technological University and from Stony Brook University (subaward 2105003Z8) acknowledge support from National Science Foundation award AGS-2133229. A. Kostinski, S. Krueger, R. Shaw, and F. Yang accomplished some of this work during a visit at the Kavli Institute for Theoretical Physics as part of the Multiphase Flows in Geophysics and the Environment program. KITP is supported in part by National Science Foundation under grant number PHY-1748958. We also want to thank Dr. Ken Cooper for the constructive discussion and for providing feedback to the manuscript.

586

Reference

588

589   Acquistapace, C., Kneifel, S., Löhnert, U., Kollias, P., Maahn, M., and Bauer-Pfundstein, M.:
590   Optimizing observations of drizzle onset with millimeter-wavelength radars, Atmospheric
591   Measurement Techniques, 10, 1783-1802, 2017.
592   Battan, L. J.: Radar observation of the atmosphere, 1973.
593   Beals, M. A., Fugal, J. P., Shaw, R. A., Lu, J., Spuler, S. M., and Stith, J. L.: Holographic
594   measurements of inhomogeneous cloud mixing at the centimeter scale, Science, 350, 87-90,
595   2015.
596   Beard, K. V., and Ochs III, H. T.: Warm-rain initiation: An overview of microphysical mechanisms,
597   Journal of Applied Meteorology and Climatology, 32, 608-625, 1993.
598   Chandrakar, K., Cantrell, W., Kostinski, A., and Shaw, R.: Data supporting the paper" Dispersion
599   aerosol indirect effect in turbulent clouds: laboratory measurements of effective radius", 2018.
600   Chandrakar, K. K., Saito, I., Yang, F., Cantrell, W., Gotoh, T., and Shaw, R. A.: Droplet size
601   distributions in turbulent clouds: Experimental evaluation of theoretical distributions, Quarterly
602   Journal of the Royal Meteorological Society, 146, 483-504, 2020.
603   Chang, K., Bench, J., Brege, M., Cantrell, W., Chandrakar, K., Ciochetto, D., Mazzoleni, C.,
604   Mazzoleni, L., Niedermeier, D., and Shaw, R.: A laboratory facility to study gas–aerosol–cloud
605   interactions in a turbulent environment: The Π chamber, Bulletin of the American Meteorological
606   Society, 97, 2343-2358, 2016.
607   Comstock, K. K., Wood, R., Yuter, S. E., and Bretherton, C. S.: Reflectivity and rain rate in and
608   below drizzling stratocumulus, Quarterly Journal of the Royal Meteorological Society: A journal
609   of the atmospheric sciences, applied meteorology and physical oceanography, 130, 2891-2918,
610   2004.
611   Cooper, K. B., and Chattopadhyay, G.: Submillimeter-wave radar: Solid-state system design and
612   applications, IEEE microwave magazine, 15, 51-67, 2014.
613   Desai, N., Chandrakar, K. K., Chang, K., Cantrell, W., and Shaw, R.: Influence of microphysical
614   variability on stochastic condensation in a turbulent laboratory cloud, Journal of the Atmospheric
615   Sciences, 75, 189-201, 2018.
616   Falkovich, G., Stepanov, M. G., and Vucelja, M.: Rain initiation time in turbulent warm clouds,
617   Journal of applied meteorology and climatology, 45, 591-599, 2006.
618   Feingold, G., Cotton, W. R., Kreidenweis, S. M., and Davis, J. T.: The impact of giant cloud
619   condensation nuclei on drizzle formation in stratocumulus: Implications for cloud radiative
620   properties, Journal of the atmospheric sciences, 56, 4100-4117, 1999.
621   Frisch, A., Fairall, C., and Snider, J.: Measurement of stratus cloud and drizzle parameters in ASTEX
622   with a Kα-band Doppler radar and a microwave radiometer, Journal of the Atmospheric Sciences,
623   52, 2788-2799, 1995.
624   Fugal, J., and Shaw, R.: Cloud particle size distributions measured with an airborne digital in-line
625   holographic instrument, Atmospheric Measurement Techniques, 2, 259-271, 2009.
626   Johnson, D. B.: The role of giant and ultragiant aerosol particles in warm rain initiation, Journal
627   of Atmospheric Sciences, 39, 448-460, 1982.

Kollias, Clothiaux, E., Miller, M., Albrecht, B., Stephens, G., and Ackerman, T.: Millimeter-wavelength radars: New frontier in atmospheric cloud and precipitation research, Bulletin of the American Meteorological Society, 88, 1608-1624, 2007.

Kollias, Remillard, J., Luke, E., and Szyrmer, W.: Cloud radar Doppler spectra in drizzling stratiform clouds: 1. Forward modeling and remote sensing applications, Journal of Geophysical Research-Atmospheres, 116, 10.1029/2010jd015237, 2011.

Kollias, Clothiaux, E. E., Ackerman, T. P., Albrecht, B. A., Widener, K. B., Moran, K. P., Luke, E. P., Johnson, K. L., Bharadwaj, N., and Mead, J. B.: Development and applications of ARM millimeter-wavelength cloud radars, Meteorological Monographs, 57, 17.11-17.19, 2016.

Kostinski, A. B., and Shaw, R. A.: Fluctuations and luck in droplet growth by coalescence, Bulletin of the American Meteorological Society, 86, 235-244, 2005.

Krueger, S. K., and Kerstein, A. R.: An economical model for simulating turbulence enhancement of droplet collisions and coalescence, Journal of Advances in Modeling Earth Systems, 10, 1858-1881, 2018.

Krueger, S. K.: Equilibrium droplet size distributions in a turbulent cloud chamber with uniform supersaturation, 2020.

Liu, Y., Geerts, B., Miller, M., Daum, P., and McGraw, R.: Threshold radar reflectivity for drizzling clouds, Geophysical research letters, 35, 2008.

Pinsky, and Khain, A.: Turbulence effects on droplet growth and size distribution in clouds—A review, Journal of aerosol science, 28, 1177-1214, 1997.

Pruppacher, H. R., and Klett, J. D.: Microphysics of Clouds and Precipitation: Reprinted 1980, Springer Science & Business Media, 2012.

Saito, I., Gotoh, T., and Watanabe, T.: Broadening of cloud droplet size distributions by condensation in turbulence, Journal of the Meteorological Society of Japan. Ser. II, 2019.

Schmidt, J. M., Flatau, P. J., Harasti, P. R., Yates, R. D., Littleton, R., Pritchard, M. S., Fischer, J. M., Fischer, E. J., Kohri, W. J., and Vetter, J. R.: Radar observations of individual rain drops in the free atmosphere, Proceedings of the National Academy of Sciences, 109, 9293-9298, 2012.

Shaw, R. A.: Particle-turbulence interactions in atmospheric clouds, Annual Review of Fluid Mechanics, 35, 183-227, 2003.

Shaw, R. A., Cantrell, W., Chen, S., Chuang, P., Donahue, N., Feingold, G., Kollias, P., Korolev, A., Kreidenweis, S., and Krueger, S.: Cloud–aerosol–turbulence interactions: Science priorities and concepts for a large-scale laboratory facility, Bulletin of the American Meteorological Society, 101, E1026-E1035, 2020.

Shaw, R. A., Thomas, S., Prabhakaran, P., Cantrell, W., Ovchinnikov, M., and Yang, F.: Fast and slow microphysics regimes in a minimalist model of cloudy Rayleigh-B\'enard convection, Physical Review Research, 5, 043018, 10.1103/PhysRevResearch.5.043018, 2023.

Thomas, S., Yang, F., Ovchinnikov, M., Cantrell, W., and Shaw, R. A.: Scaling of turbulence and microphysics in a convection–cloud chamber of varying height, Journal of Advances in Modeling Earth Systems, 15, e2022MS003304, 2023.

Wood: Stratocumulus Clouds, Monthly Weather Review, 140, 2373-2423, 10.1175/mwr-d-11-00121.1, 2012.

Yau, M. K., and Rogers, R. R.: A short course in cloud physics, Elsevier, 1996.

670   Zhu, Z., Kollias, P., Luke, E., and Yang, F.: New insights on the prevalence of drizzle in marine

671   stratocumulus clouds based on a machine learning algorithm applied to radar Doppler spectra,

672   Atmospheric Chemistry and Physics, 22, 7405-7416, 2022.

673